



**HAL**  
open science

## Improving tool wear and surface covering in polishing via toolpath optimization

Julien Chaves-Jacob, Jean-Marc Linares, Jean-Michel Sprael

► **To cite this version:**

Julien Chaves-Jacob, Jean-Marc Linares, Jean-Michel Sprael. Improving tool wear and surface covering in polishing via toolpath optimization. *Journal of Materials Processing Technology*, 2013, 213, pp.1661 - 1668. 10.1016/j.jmatprotec.2013.04.005 . hal-01440252

**HAL Id: hal-01440252**

**<https://amu.hal.science/hal-01440252>**

Submitted on 19 Jan 2017

**HAL** is a multi-disciplinary open access archive for the deposit and dissemination of scientific research documents, whether they are published or not. The documents may come from teaching and research institutions in France or abroad, or from public or private research centers.

L'archive ouverte pluridisciplinaire **HAL**, est destinée au dépôt et à la diffusion de documents scientifiques de niveau recherche, publiés ou non, émanant des établissements d'enseignement et de recherche français ou étrangers, des laboratoires publics ou privés.

# Improving tool wear and surface covering in polishing via toolpath optimization

Julien Chaves-Jacob<sup>\*</sup>, Jean-Marc Linares, Jean-Michel Sprael

Aix-Marseille Université, CNRS, ISM UMR 7287, 13288 Marseille cedex 09, France

Polishing operations are commonly carried out manually, thus inducing variability on the surface quality. The aim of this paper is to automate the polishing of free-form surfaces in order to obtain high quality surfaces. Tool wear and toolpath surface covering have a great impact on surface properties. The current work proposes therefore a toolpath which optimizes both tool wear and surface covering. This toolpath is composed of an optimized elementary pattern repeated along a 5-axis carrier trajectory. Usually, trochoid patterns are used. Non uniform wear of the tool and uneven probability density function of the surface covering are the main inconvenients of such pattern. So, this paper proposes two optimized patterns: Spade and Triangular. Both of them lead to uniform tool wear. Our paper also demonstrates that the second solution provides a uniform probability density function. All presented computations are validated experimentally.

Keywords: Polishing Biomedical Precision Surface Toolpath Optimization

## 1. Introduction

Biomedical implants need a high finishing quality, in particular for the roughness of friction surfaces. Femoral parts of knee prostheses hold these problems. Manufacturing of such workpiece attracts the interest of different research teams in the world. [Hilerio et al. \(2004\)](#) present the Product Life Management of knee prostheses and a study of the polishing stages. The manufacturing process of this biomedical part is presented in [Fig. 1](#). First, the kinematic and functional requirements are specified in the Computer Aided Design (CAD) model. Next, due to the fact that implants are commonly realized in cobalt-chrome alloy, difficult to machine, lost-wax casting is generally selected to obtain the rough of geometry. Sometimes, before starting polishing, a rough-machined is also realized. Following, the prosthesis is polished with a succession of abrasive tools. After manufacturing, the implant undergoes many cleanings and sterilizations.

In the implant process planning, polishing operations are critical and correspond to the longest phases of the finish process. This stage needs accurate positioning of the prosthesis to the abrasive tool. For that reason it remains commonly still manual. This problem is recurrent for a great number of types of parts like molds, die sets, flow components (impellers, inducers, etc.), biomedical implants (knee, hip, etc.), etc. Polishing operations are however needed to obtain the required finish quality. These stages are labor

intense and dangerous to health of the operator. Indeed, small metal airborne particles are produced by this process and may be inspired by the operator. [Lison et al. \(1996\)](#) present a study to understand the pathogenesis of lung disease produced by cobalt airborne particles (standard alloy used for prostheses). Furthermore, the geometrical result is greatly depending on the skill of the operator. Therefore, many works try to automate the polishing operation to stabilize the implant quality and reduce the production costs. The first problem is to find a machine able to emulate hand movements. Some special machines have been designed by numerous research teams. For example, [Lee et al. \(2001\)](#) developed a 2-axis robot designed to be mounted on a 3-axis CNC machine. For polishing assistance, [Hocheng and Kuo \(2002\)](#) propose a specific machine using ultrasonic axial vibrations of the tool. [Wu et al. \(2007\)](#) used a grinding center with an elastic ball end tool to polish free-form surfaces. [Charlton and Blunt \(2008\)](#) designed an industrial 7-axis machine dedicated to polishing operations. [Liao et al. \(2008\)](#) present a compliant toolhead for polishing and deburring operations. The presented head is mounted on a robotized tripod. [Hung et al. \(2011\)](#) suggest the use of a 'rock-and-roll' polishing toolpath strategy to get homogeneous tool wear. The presented method uses a ball-tool in rotation around the tool-axis. Furthermore, an additional rotation around the center of the ball-tool is applied to homogenize the tool wear along the spherical surface.

These machines are however only dedicated to polishing operations. In the same way, the use of 5 and 6-axis common industrial robots has been proposed. The advantage of this solution is its low cost. Moreover, the degrees of freedom of the robot offer a great accessibility to any free form surface. However, the accuracy of such

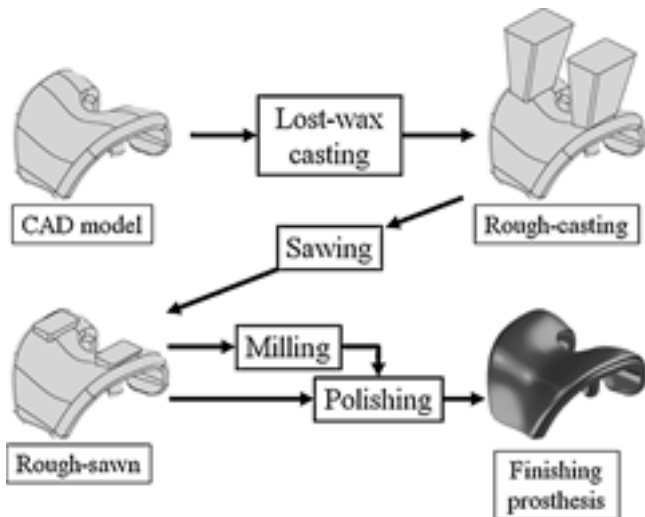


Fig. 1. Process planning of a knee prosthesis femoral part.

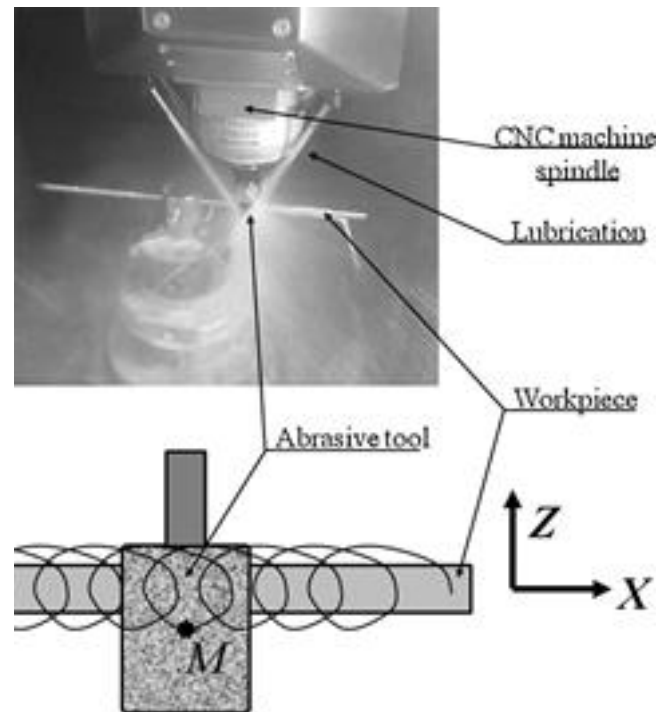


Fig. 2. Polishing process on a 5-axis milling machine.

machine is limited to about 0.1 mm. The use of a machine dedicated to polishing imposes preparing the surfaces with 5-axis milling. In such process planning, polishing problems may then appear due to the loss of reference frame of the workpiece during its dismounting and next mounting. Thus, [Denkena et al. \(2010\)](#) suggest the use of one single CNC machine for both rough milling and polishing. In fact, such process planning is the most accurate way to know the localization of the real geometry before polishing.

The major problem of automated polishing is the control of the contact pressure between the tool and the workpiece. This pressure is essential in the material removal rate. To monitor this pressure, it is necessary to control the surface geometry and the contact force between the tool and the surface. Using a CNC machine, the workpiece is not dismantled between rough and polishing stages. In consequence, the polished surface geometry is accurately controlled. Two methods are employed to monitor the contact force:

- Using a load cell to control the force applied to the workpiece. The penetration of the tool is then directly linked to the selected force. [Tsai and Huang \(2006\)](#) control the load applied to a compliance tool using a polishing force control loop. [Nagata et al. \(2007\)](#) employ an industrial robot driven in force to polish molds. [Huissoon et al. \(2002\)](#) propose to polish surfaces with a flexible abrasive disk mounted on a load cell. This sensor is used to drive the tool position in force.
- Defining the constitutive law characterizing the relation between the tool displacement and the contact force. This law can be obtained through an experimental approach or theoretical calculations. [Tsai and Huang \(2006\)](#) use a polishing experiment, instrumented with a load cell to determine this law. On the other hand, lots of studies propose a Hertz contact model to determine the constitutive law between the tool displacement and the contact force. For example, [Roswell et al. \(2006\)](#) implement this model to find the stress in the Hertz contact between the tool and the polished surface.

Another problem is to define the polishing toolpath. Its aim is to cover the entire surface. To solve this problem, [Tam et al. \(1999\)](#) propose a linear scanning of the parametric space of the surface. After, the authors optimize the steps between the different scanning toolpath segments to get a uniform covering of the surface. This method reduces the overlapping of the segments, thus lowering their number. To boost the overlapping, [Márquez et al. \(2005\)](#) propose to use an elementary square pattern with two diagonals.

Furthermore, fractal curves can be employed to cover the entire surface. Commonly Hilbert's curves are therefore taken. [Chen et al. \(2002\)](#) propose a method to compute Hilbert's curves on complex surfaces. In this paper, the authors test this method on a large range of geometries. [Pessoles and Tournier \(2009\)](#) use Hilbert's curves as a carrier to generate polishing toolpaths. The surface covering may be resolved using an elementary pattern repeated along a carrier toolpath. Usually, a trochoid pattern is selected, because the related movement looks like human polishing trajectory. For example, [Tsai and Huang \(2006\)](#) used a trochoid pattern in polishing toolpaths along a linear carrier toolpath. This type of pattern leads to a great number of loops which many times cross the same surface area. The trochoid pattern gives interesting results but its choice is arbitrary.

The aim of current paper is now to propose different toolpaths to automate the polishing operations of workpieces. A mathematical optimization of the polishing toolpath pattern will thus be presented to get homogeneous tool wearing and uniform surface covering. In a first section, the employed polishing process will be detailed. Next, the tool wear induced by trochoid patterns in flank polishing will be analyzed. This study will highlight the non uniform wear of the tool using such pattern. After, a Spade pattern will be proposed to correct this problem. Subsequently, a similar approach will be used to get a pattern which leads to a uniform covering of the polished surface. The results of experiments carried out to demonstrate the relevance of the presented developments will finally be presented.

## 2. Polishing process on CNC

The proposed polishing toolpaths can be used on any 5-axis CNC machine or industrial robot. The defined experimental process is illustrated in [Fig. 2](#). The polishing operation is carried out using the flank of a cylindrical abrasive tool.

The proposed 5-axis polishing toolpath is a repetition of elementary loops with a small feed movement. This movement is presented in [Fig. 3](#). The polishing toolpath is composed of a carrier toolpath and an elementary pattern along the tool axis. First,

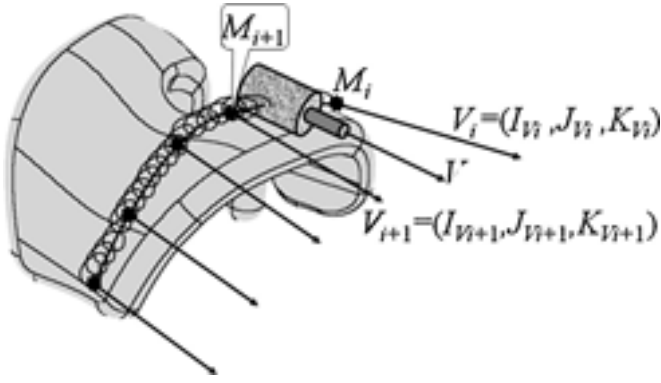


Fig. 3. Polishing toolpath computation.

the carrier toolpath is computed using a simple linear interpolation. It is composed of a set of points  $M_i$ , which may be computed using an industrial Computer Aided Manufacturing (CAM) system. After, a five degree polynomial interpolation, as presented by Chaves-Jacob et al. (2009), is used to smooth the carrier toolpath and get a trajectory with continuous slopes and curvatures. Nevertheless, with this polynomial interpolation, all the points  $M_i$  still lie on the smoothed toolpath. Eq. (1) presents the expression of this polynomial interpolation. In these relations, the parameter  $u_{\text{polynomial}}$  defining the position of a point along the 3D carrier trajectory is a normalized factor varying from 0 to 1.

$$\begin{aligned} X_{\text{carrier}} &= a_0 + a_1 \cdot u_{\text{polynomial}} + a_2 \cdot u_{\text{polynomial}}^2 + a_3 \cdot u_{\text{polynomial}}^3 + a_4 \cdot u_{\text{polynomial}}^4 + a_5 \cdot u_{\text{polynomial}}^5 \\ Y_{\text{carrier}} &= b_0 + b_1 \cdot u_{\text{polynomial}} + b_2 \cdot u_{\text{polynomial}}^2 + b_3 \cdot u_{\text{polynomial}}^3 + b_4 \cdot u_{\text{polynomial}}^4 + b_5 \cdot u_{\text{polynomial}}^5 \\ Z_{\text{carrier}} &= c_0 + c_1 \cdot u_{\text{polynomial}} + c_2 \cdot u_{\text{polynomial}}^2 + c_3 \cdot u_{\text{polynomial}}^3 + c_4 \cdot u_{\text{polynomial}}^4 + c_5 \cdot u_{\text{polynomial}}^5 \end{aligned} \quad (1)$$

Between two consecutive points,  $M_i$  and  $M_{i+1}$ , of the smoothed carrier toolpath, the polishing toolpath is then computed. It is composed of elementary patterns, repeated  $N$  times between points  $M_i$  and  $M_{i+1}$ . In a first time, the pattern curve is defined in a 2D space,  $(U_1, U_2)$  in Fig. 4.  $M$  is the current point of the pattern. It is defined by the coordinates  $U_{1M}(u_{\text{pattern}})$  and  $U_{2M}(u_{\text{pattern}})$ . The pattern curve is thus described by a parameter  $u_{\text{pattern}}$ , varying from 0 to  $N$ . Each loop induces a feed progression of parameter  $a$  in the 2D space. In this study, the elementary patterns were based on trochoid curves. Eq. (2) presents the coordinates  $U_{1M}(u_{\text{pattern}})$  and  $U_{2M}(u_{\text{pattern}})$  for such trochoid patterns.

$$\begin{aligned} U_{1M}(u_{\text{pattern}}) &= R \cdot [1 - \cos(2 \cdot u_{\text{pattern}})] + a \cdot u_{\text{pattern}} \\ U_{2M}(u_{\text{pattern}}) &= -R \cdot \sin(2 \cdot u_{\text{pattern}}) \end{aligned} \quad (2)$$

The elementary patterns are driven by four parameters. Two parameters,  $R$  and  $a$ , define the pattern geometry:  $R$  is the half amplitude of the tool in its axial direction and  $a$  is the 2D longitudinal feed progression by loop. Fig. 5 presents the 6 possible morphologies of the elementary trochoid pattern. This morphology depends on the ratio of  $R$  and  $a$ . For polishing patterns, the value of  $R$  is usually selected greater than  $a$  to be in the first three cases of Fig. 5. The two other parameters define the density of the pattern along the carrier toolpath. They consist of the number  $N$  of

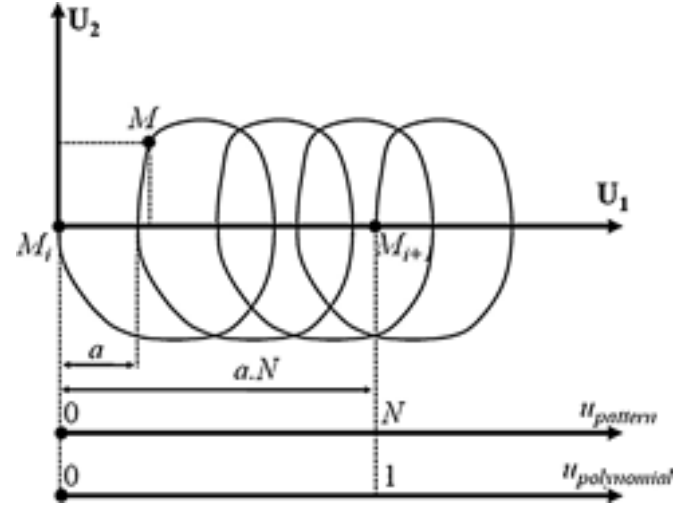


Fig. 4. Elementary pattern in a 2D space.

loops between two consecutive points of the carrier toolpath ( $M_i$  and  $M_{i+1}$ ) and the distance between these two points.

The polishing pattern, first defined in a 2D space, is then projected to the 3D carried toolpath. For that purpose, the variable  $u_{\text{polynomial}}$  defining the coordinate of the tool along the carrier trajectory is derived from the position  $U_{1M}(u_{\text{pattern}})$  in the 2D diagram, using following Eq. (3).

$$u_{\text{polynomial}} = \frac{U_{1M}(u_{\text{pattern}})}{a \cdot N} \quad (3)$$

This link between the 2D space of the elementary patterns driven by  $u_{\text{pattern}}$  and the 3D parameter  $u_{\text{polynomial}}$  is also shown at the bottom of Fig. 4. The additional oscillating movement of the tool, in the direction of the rotation axis corresponds just to the displacement  $U_{2M}(u_{\text{pattern}})$  as defined in the 2D diagram.

The next step is the computation of the inclination of the tool throughout the carrier toolpath trajectory. A simple linear interpolation of the components  $(I; J; K)$  of the tool axis direction vectors ( $V_i; V_{i+1}$ ), defined by the CAM system, for points  $M_i$  and  $M_{i+1}$  is used for that purpose (Eq. (4)). Fig. 3 illustrates the used notation for the tool axes computation.

$$V = (1 - u_{\text{polynomial}}) \cdot V_i + u_{\text{polynomial}} \cdot V_{i+1} = (I_V; J_V; K_V) \quad (4)$$

Thereafter, the 3D polishing toolpath is computed using Eq. (5). This equation is obtained moving the tool along its axis to describe the elementary pattern loops. This polishing toolpath is decomposed into small linear steps and then smoothed using a five degree polynomial interpolation. To finish, the CNC code is generated by the developed program. The polishing toolpath thus obtained is



Fig. 5. Morphologies of the elementary patterns.

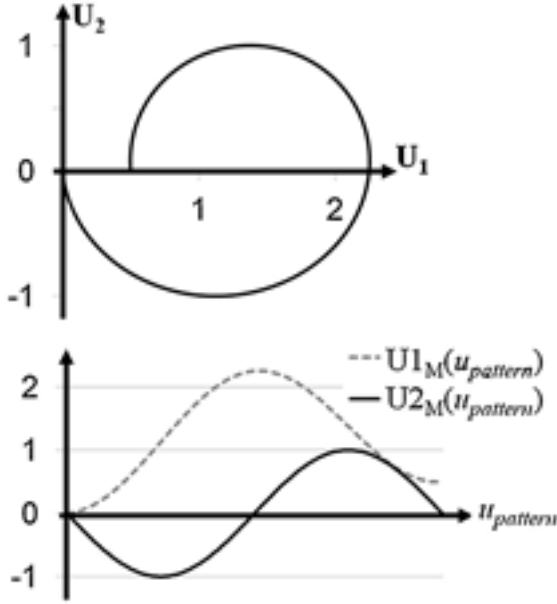


Fig. 6. Example of trochoid pattern.

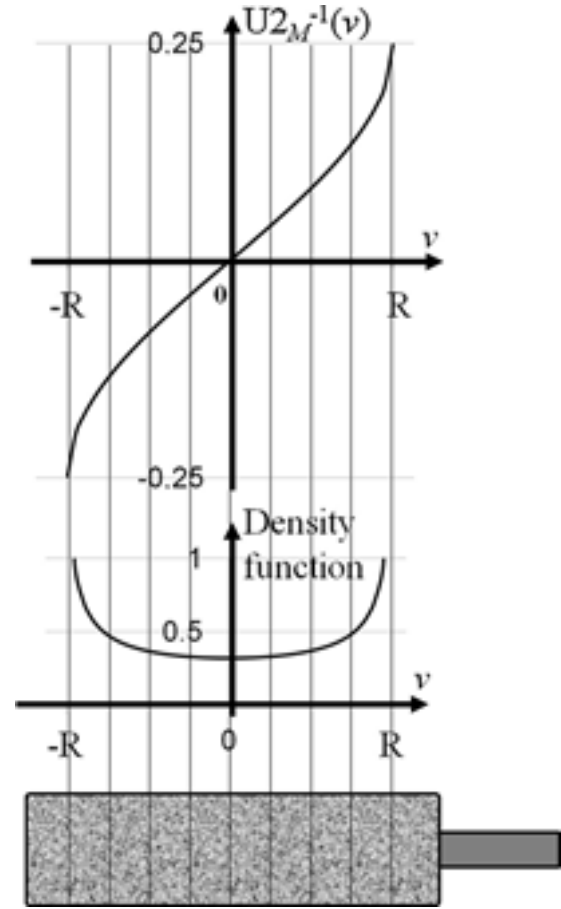


Fig. 7. Tool wear PDF using a trochoid pattern.

continuous in position, slope and curvature. Eq. (6) presents one line of the CNC program for a SIEMENS 840D. In this equation,  $(X_p, Y_p, Z_p)$  are the end point coordinates of the line and  $a_i, b_i$  and  $c_i$  are the coefficients of the five degree polynomial curve of the toolpath. The coefficients  $a_0, a_1, b_0, b_1, c_0$  and  $c_1$  are not provided in the program since they are directly linked to the current and end coordinates, and are thus computed by the CNC machine.

$$\begin{aligned}
 X_M &= a_0 + a_1 \cdot u_{\text{polynomial}} + a_2 \cdot u_{\text{polynomial}}^2 + a_3 \cdot u_{\text{polynomial}}^3 + a_4 \cdot u_{\text{polynomial}}^4 + a_5 \cdot u_{\text{polynomial}}^5 + U2_M(u_{\text{pattern}}) \cdot I_v \\
 Y_M &= b_0 + b_1 \cdot u_{\text{polynomial}} + b_2 \cdot u_{\text{polynomial}}^2 + b_3 \cdot u_{\text{polynomial}}^3 + b_4 \cdot u_{\text{polynomial}}^4 + b_5 \cdot u_{\text{polynomial}}^5 + U2_M(u_{\text{pattern}}) \cdot J_v \\
 Z_M &= c_0 + c_1 \cdot u_{\text{polynomial}} + c_2 \cdot u_{\text{polynomial}}^2 + c_3 \cdot u_{\text{polynomial}}^3 + c_4 \cdot u_{\text{polynomial}}^4 + c_5 \cdot u_{\text{polynomial}}^5 + U2_M(u_{\text{pattern}}) \cdot K_v \\
 \text{POLY X} &= \text{PO}(X_p, a_2, a_3, a_4, a_5)Y = \text{PO}(Y_p, b_2, b_3, b_4, b_5)Z \\
 &= \text{PO}(Z_p, c_2, c_3, c_4, c_5)PL = 1
 \end{aligned} \tag{6}$$

### 3. Optimization of the tool wear

#### 3.1. Non uniform tool wear with trochoid patterns

In a first time, an elementary trochoid pattern is studied to highlight the difference of wear along the tool axis. The trochoid pattern is defined by Eq. (2) and the example, corresponding to the parameters  $R = 1$  and  $a = 0.5$ , is presented in Fig. 6.

In our polynomial interpolations, it is the parameter  $u_{\text{pattern}}$  which is used to drive the CNC axes. This variable is thus directly linked to the system clock and therefore proportional to time. For that reason, the wear of any axial point of the tool just depends on the whole time spent at a given position  $U2_M$  in the toolpath. Due to the symmetry of the movement, only a half period of the trochoid pattern had to be studied (Eq. (7)). To define the probability density function (PDF) along the tool axis it is then necessary to inverse this function. The inverse function of  $U2_M$  is presented in Eq. (8) and at the top of Fig. 7.

$$\begin{aligned}
 u_{\text{pattern}} &\in [-0.25; 0.25] \\
 U2_M(u_{\text{pattern}}) &= -R \cdot \sin(2 \cdot u_{\text{pattern}})
 \end{aligned} \tag{7}$$

$$\begin{aligned}
 v &\in [-R; R] \\
 U2_M^{-1}(v) &= \frac{1}{2} \cdot \arcsin \frac{v}{R}
 \end{aligned} \tag{8}$$

The PDF of the wear is finally computed by deriving and normalizing Eq. (8). This leads to the expression given in Eq. (9). The PDF is plotted in Fig. 7. It expresses the time ratio spent by any tool point at the same given axial polishing position. Its value is directly linked to the wear of the tool. As clearly shown by Fig. 7, a significant share of the polishing time relates to the two end points of the tool. This obviously demonstrates that trochoid patterns lead to non uniform wear of the tool.

$$\begin{aligned}
 v &\in [-R; R] \\
 \frac{d(U2_M^{-1}(v))}{dv} &= \frac{1}{R} \cdot \frac{1}{\sqrt{1 - (v/R)^2}}
 \end{aligned} \tag{9}$$

#### 3.2. Uniform tool wear with Spade patterns

Section 3.1 demonstrated that trochoid patterns induce an intensified wear of the two tool end points. In this section, a Spade pattern will be presented to correct this wear problem. To obtain a homogeneous wear of the tool, it is obviously necessary to get a uniform PDF along the tool axis (Eq. (10)). This distribution leads to

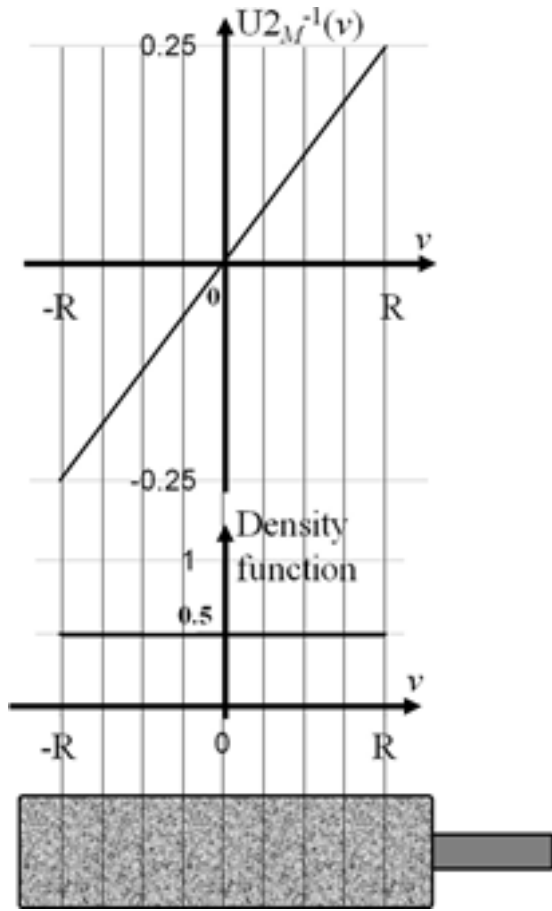


Fig. 8. Tool wear PDF using a Spade pattern.

a linear expression of  $U2_M^{-1}$  (Eq. (11)). Fig. 8 shows the wear density function of the Spade pattern.

$$v \in [-R; R] \quad (10)$$

$$\frac{d(U2_M^{-1}(v))}{dv} = \frac{1}{2R}$$

$$v \in [-R; R]$$

$$U2_M^{-1}(v) = \frac{1}{4R} \cdot v \quad (11)$$

After, the loop parameters selected for the trochoid patterns were preserved to compute the wear optimized toolpath, presented in Eq. (12). The shape of the related elementary pattern, presented in Fig. 9, looks like a Spade.

$$U2_M(u_{pattern}) = -4R \cdot (u_{pattern} + 0.5) \quad \text{if } u_{pattern} \in [-0.5; -0.25]$$

$$U2_M(u_{pattern}) = 4R \cdot u_{pattern} \quad \text{if } u_{pattern} \in [-0.25; 0.25] \quad (12)$$

$$U2_M(u_{pattern}) = -4R \cdot (u_{pattern} - 0.5) \quad \text{if } u_{pattern} \in [0.25; 0.5]$$

#### 4. Optimization of the covering

Section 3 presented a Spade pattern, distorting the trochoid pattern, to obtain homogeneous wear of the tool, along its axis. The same type of optimization is now applied to this polishing toolpath to get a uniform surface covering. For that purpose, the elementary patterns must have a uniform PDF in the two main directions ( $U1$ ,  $U2$ ) of displacement. However, since the two components ( $U1$ ,  $U2$ ) are independent variables, the joint surface PDF corresponds to the product of two independent functions, thus allowing separated optimization. In Section 3, the trochoid pattern was already

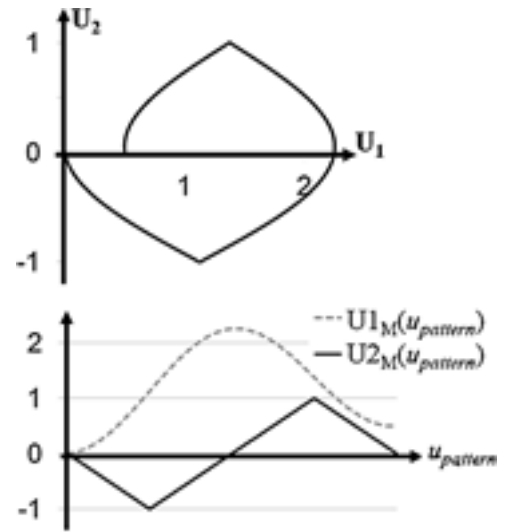


Fig. 9. Wear optimized patterns, Spade toolpath.

distorted in direction  $U2$  to get a uniform PDF of this variable. Now, the density of the pattern has to be optimized in direction  $U1$ .

##### 4.1. Elementary trochoid pattern covering study

The coordinate  $U1_M$  of the trochoid pattern is therefore analyzed. Due to the symmetry of the displacement, just a half period is considered for  $u_{pattern} \in [0; 0.5]$  in Eq. (2). Its PDF is presented in Eq. (13) and Fig. 10. It shows that, the trochoid pattern induces a non uniform covering in direction  $U1$ . Fig. 10 highlights that the trochoid pattern leads to a larger covering at the beginning and the end of the studied interval which corresponds to the center positions of the tool.

$$v \in [0; 2R + \frac{a}{2}] \quad (13)$$

$$\frac{d(U1_M^{-1}(v))}{dv} = \frac{1}{N \cdot (2R \cdot \sin(2 \cdot u_{pattern}) + a)}$$

$$\text{with } v = R \cdot [1 - \cos(2 \cdot u_{pattern})] + a \cdot u_{pattern} \quad \text{where } u_{pattern} \in [0; 0.5]$$

##### 4.2. Covering optimization

To get a homogeneous covering of the surface, a uniform PDF of the elementary pattern has to be obtained in direction  $U1$ . This gives the relationships of Eq. (14). The oscillating amplitude,  $2R$ , and the

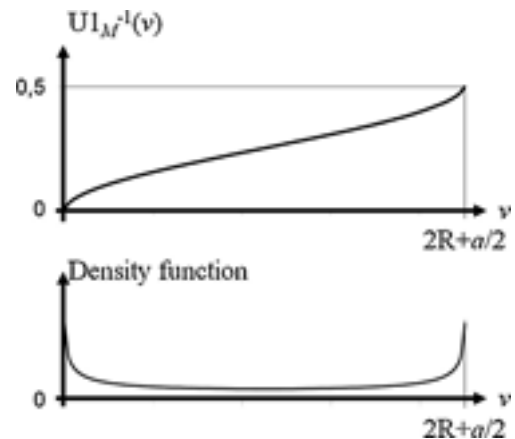


Fig. 10. PDF of the trochoid pattern in  $U1$  direction.

	Elementary pattern	Covering
Trochoid		
Spade		
Triangular		

Fig. 11. Surface covering of the three elementary patterns.

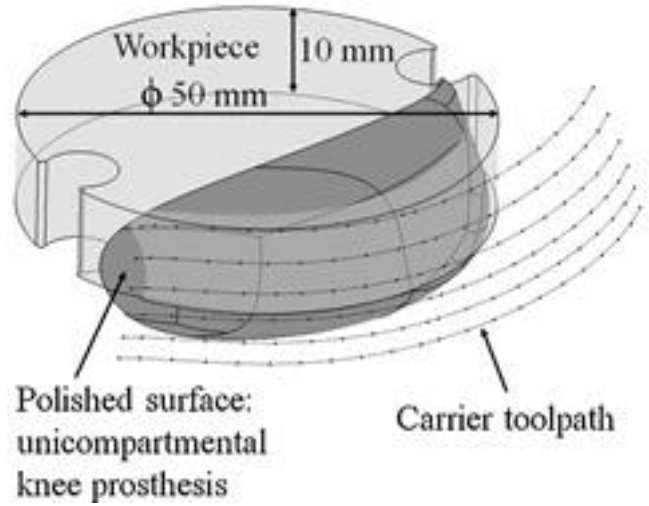


Fig. 12. Polished surface.

feed  $a$  of the elementary trochoid pattern are however preserved, thus leading to the optimized expression of  $U1_M$  presented in Eq. (15). The resulting pattern is named Triangular pattern.

$$u_{\text{pattern}} \in [0; 0.5] \quad (14)$$

$$v \in [0; 2R + a/2]$$

$$d(U1_M^{-1}(v))/dv = 1 / N \cdot (4R + a)$$

$$U1_M(u_{\text{pattern}}) = 4R \cdot u_{\text{pattern}} + a \cdot u_{\text{pattern}} \quad \text{if } u_{\text{pattern}} \in [0; 0.5] \quad (15)$$

$$U1_M(u_{\text{pattern}}) = -4R \cdot (u_{\text{pattern}} - 1) + a \cdot u_{\text{pattern}} \quad \text{if } u_{\text{pattern}} \in [0.5; 1]$$

The 3 types of elementary patterns are presented in Fig. 11. This figure highlights the homogeneous covering of the Triangular optimized pattern. Fig. 11 also synthesizes the steps of the trochoid pattern optimization. The optimization of the trochoid pattern by the Triangular pattern can surprise the reader because this pattern induces slope discontinuities. In reality, these discontinuities are suppressed by the five degree polynomial smoothing applied to the polishing toolpath. The presented developments have been experimentally tested and provided interesting results.

## 5. Experimental validation

Fig. 12 presents the CAD model of the workpiece used for the experimental validation. The polished surface is a part of friction surface of unicompartmental knee prostheses. First, the surface is rough machined with a flat end mill. Next an abrasive ball tool is used to semi-finishing. A polynomial toolpath is therefore used to reduce the surface irregularities. The finishing is realized with a polishing tool composed of emery grain (size around 50 mm) linked by a supple rubber. The geometry of the polishing tool is a cylinder of 32 mm in diameter and height. During the polishing operation, lubricant is employed. The flow used is a grinding lubricant with a low fat content and a pressure of around 5 bars. The surface is polished using the six carrier toolpaths presented in Fig. 12. The polishing patterns have a radius  $R$  of 12 mm and a feed  $a$  of 6 mm. The polishing toolpath is computed to have one loop per 2.5 mm.

To highlight the non uniform wear of the tool and the surface covering, three surfaces were polished. The first is polished with the trochoid pattern, the second with the Spade and the third with a Triangular toolpath. Fig. 13 presents the three employed tools and the measured profiles along the tool axes. These profiles are

accurately characterized through optical measurements using a chromatic confocal sensing CMM. The resolution of this CMM is about 10 nm. The profiles are measured along all the active part of the tool. An example of result is shown in Fig. 13. The vertical lines at the end of the measured profiles correspond to the extremities of the tool. As expected (see Section 3.1), the tool which machined a trochoid patterns presents an over-wear at the end of the used area. On the contrary, Spade and Triangular patterns generate uniform tool wear. These measures validate the optimization of toolpath in tool wear.

Subsequently, the polished surfaces were measured on a 2 mm × 4 mm area. The length of these zones were set to the

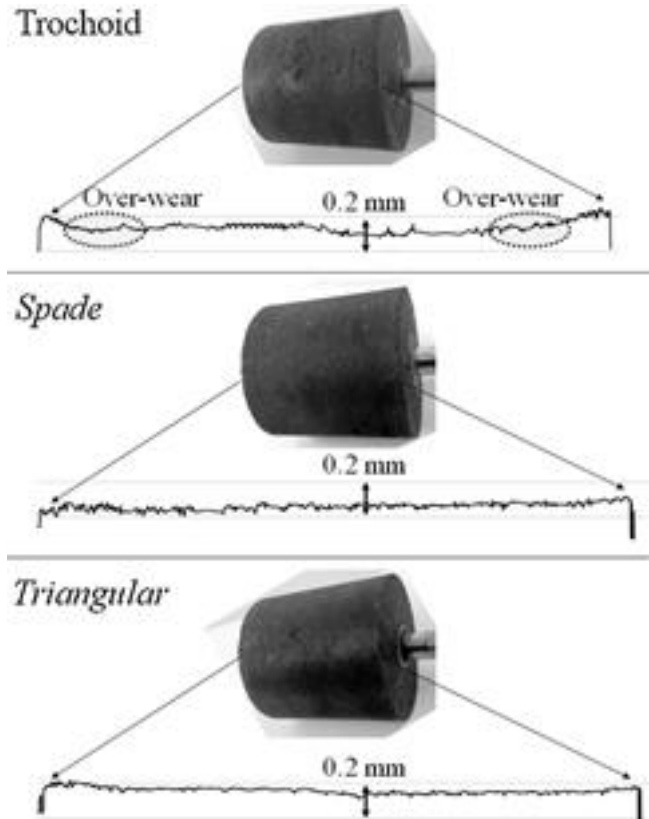


Fig. 13. Experimental tool wear profile comparison.

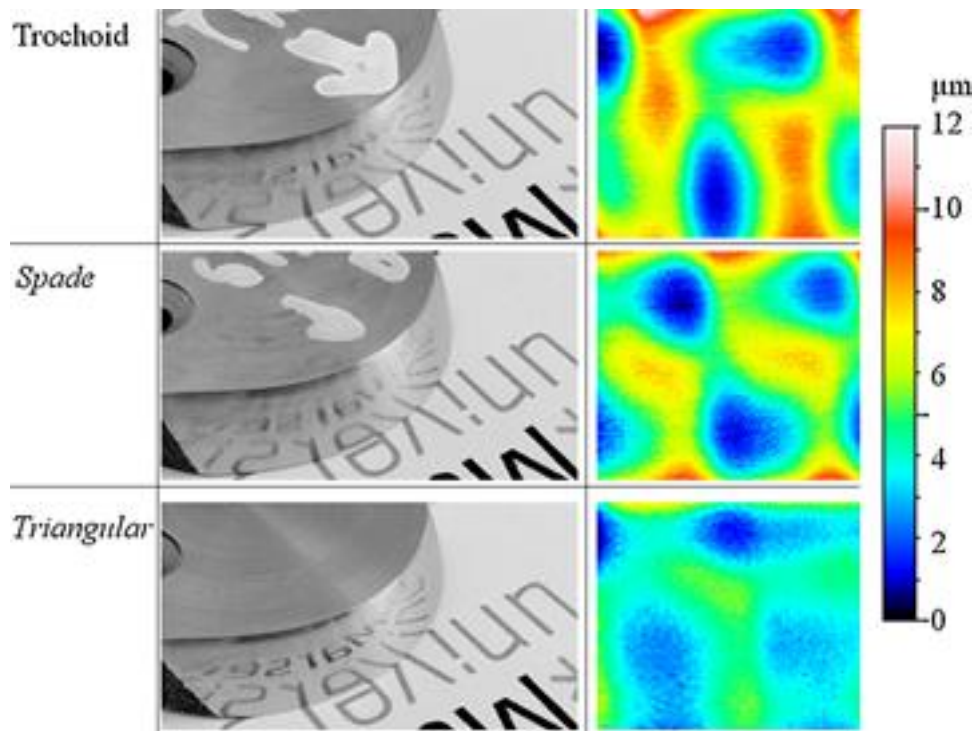


Fig. 14. Comparison of polished surfaces.

direction of the carrier toolpath and scanned with a step of 4 mm. In the other direction, the measured step was 10 mm. The measured data are then filtered by a smooth three degree polynomial in the two directions. The results of these roughness measurements are presented in the maps at the right of Fig. 14. They clearly show that triangular patterns lead to the lowest roughness amplitude. To evaluate the quality of polished surfaces it is usual to test its reflectivity using the manufactured part as a mirror for a fixed image. The left images of Fig. 14 show the result of such test. The image reflected by the surface polished with the trochoid pattern is more disturbed compared to the surface realized with the triangular toolpath. This is correlated to the roughness results. The reflection perturbations are generated by facets on the polished surface. These facets are induced by the non uniform PDF of the tool covering on the surface using trochoid or Spade patterns. The facets generated by the Spade patterns are smaller compared to those produced by the trochoid toolpath. This result can be explained by the fact that Spade patterns have been optimized in one of the two directions. Finally, Triangular patterns give the best surface quality with a uniform tool wear.

## 6. Conclusions

This paper developed an optimal toolpath for surface polishing. First a trochoid pattern was considered since it is commonly employed. In fact, this toolpath creates loops which cross many times the same surface area and its trajectory looks like human polishing movements. The aim of this current work was however to optimize the geometry of the elementary pattern to get homogeneous wear of the tool and uniform covering of the surface.

Our study has also proposed a method to compute 3D polishing toolpaths for 5-axis machines and industrial robots. The proposed method uses the flank of cylindrical abrasive tools. The toolpath was obtained adding elementary patterns on a carrier toolpath. The developed method generates a CNC program using a five degree polynomial interpolation to obtain a smooth toolpath.

Furthermore, this work has studied the tool wear by analyzing the probability density function (PDF) along the axial oscillating movement. This analysis showed that the trochoid pattern produces a heterogeneous wear of the tool. In this classical toolpath, in fact, the end points of the tool are the most loaded. Thereafter, a Spade shape pattern has therefore been proposed to generate homogeneous tool wear. Furthermore, it is also necessary to get a uniform covering of the surface. A Triangular pattern has been proposed for that purpose. Mathematical computations have thus demonstrated that this scheme is an optimal solution to obtain high surface quality. Indeed, Triangular patterns simultaneously lead to homogeneous tool wear and uniform surface covering.

Subsequently, three surfaces were polished using trochoid, Spade and Triangular patterns. The tools wear were measured after the polishing operation and corroborate the theoretical developments. Thereafter, the polished surfaces were measured with an optical CMM. The quality of the surface obtained with the Triangular pattern is significantly better in comparison to the surfaces polished with the trochoid and Spade patterns. This improvement is obtained thanks to the uniform covering PDF.

## References

- Charlton, P., Blunt, L., 2008. Surface and form metrology of polished “freeform” biological surfaces. *Wear* 264, 394–399.
- Chaves-Jacob, J., Linares, J.M., Sprauel, J.M., 2009. Increasing of surface quality in friction free-form surfaces of knee prosthesis. *CIRP Annals – Manufacturing Technology* 60, 531–534.
- Chen, C.C.A., Juang, Y.S., Lin, W.Z., 2002. Generation of fractal toolpaths for irregular shapes of surface finishing areas. *Journal of Materials Processing Technology* 127, 146–150.
- Denkena, B., De Leon, L., Turger, A., Behrens, L., 2010. Prediction of contact conditions and theoretical roughness in manufacturing of complex implants by toric grinding tools. *International Journal of Machine Tools & Manufacture* 50, 630–636.
- Hilerio, I., Mathia, T., Alepee, C., 2004. 3D measurements of the knee prosthesis surfaces applied in optimizing of manufacturing process. *Wear* 257, 1230–1234.
- Hocheng, H., Kuo, K.L., 2002. Fundamental study of ultrasonic polishing of mold steel. *International Journal of Machine Tools & Manufacture* 42, 7–13.

- Huissoon, J.P., Ismail, F., Jafari, A., Bedi, S., 2002. Automated polishing of die steel surfaces. *International Journal of Advance Manufacturing Technology* 19, 285–290.
- Hung, T.C., Chang, S.H., Hsu, S.P., Su, Y.T., 2011. Reduction of tool wear during hydrodynamic polishing: a 'rock-and-roll' polishing strategy. *Journal of Materials Processing Technology* 211, 1069–1075.
- Lee, M.C., Go, S.J., Lee, M.H., Jun, C.S., Kim, D.S., Cha, K.D., Ahn, J.H., 2001. A robust trajectory tracking control of a polishing robot system based on CAM data. *Robotics and Computer Integrated Manufacturing* 17, 177–183.
- Liao, L., Xi, F., Liu, K., 2008. Modeling and control of automated polishing/deburring process using a dual-purpose compliant toolhead. *International Journal of Machine Tools & Manufacture* 48, 1454–1463.
- Lison, D., Lauwerys, R., Demedts, M., Nemery, B., 1996. Experimental research into the pathogenesis of cobalt/hard metal lung disease. *European Respiratory Journal* 9, 1024–1028.
- Márquez, J.J., Pérez, J.M., Ríos, J., Vizán, A., 2005. Process modeling for robotic polishing. *Journal of Materials Processing Technology* 159, 69–82.
- Nagata, F., Hase, T., Haga, Z., Omoto, M., Watanabe, K., 2007. CAD/CAM-based position/force controller for a mold polishing robot. *Mechatronics* 17, 207–216.
- Pessoles, X., Tournier, C., 2009. Automatic polishing process of plastic injection molds on a 5-axis milling center. *Journal of Materials Processing Technology* 209, 3665–3673.
- Roswell, A., Xi, F., Liu, G., 2006. Modelling and analysis of contact stress for automated polishing. *International Journal of Machine Tools & Manufacture* 46, 424–435.
- Tam, H.Y., Lui, O.C., Mok, A.C.K., 1999. Robotic polishing of free-form surfaces using scanning paths. *Journal of Materials Processing Technology* 95, 191–200.
- Tsai, M.J., Huang, J.F., 2006. Efficient automatic polishing process with a new compliant abrasive tool. *International Journal of Advance Manufacturing Technology* 30, 817–827.
- Wu, X., Kita, Y., Ikoku, K., 2007. New polishing technology of free form surface by GC. *Journal of Materials Processing Technology* 187–188, 81–84.